Dimensional Reduction in II–VI Materials: $A_2Cd_3Q_4$ (A = K, Q = S, Se, Te; A = Rb, Q = S, Se), Novel Ternary Low-Dimensional Cadmium Chalcogenides Produced by Incorporation of A_2Q in CdQ

Enos A. Axtell III, Ju-Hsiou Liao, Zoe Pikramenou, and Mercouri G. Kanatzidis*

Abstract: The synthesis of the isomorphous, layered chalcogenides $K_2Cd_3S_4$ (**I**), $Rb_2Cd_3S_4$ (**II**), $K_2Cd_3Se_4$ (**III**), $Rb_2Cd_3Se_4$ (**IV**), and $K_2Cd_3Te_4$ (**V**) in molten A_2Q_x fluxes is reported (A = K, Rb; Q = S, Se, Te; x = 2 to 3). The compounds form as $(Cd_3Q_4)_n^{2n-}$ layers interspersed with A^+ cations; the layers are composed of $Cd_3Q_4^{2-}$ units shaped as truncated cubes. The compounds have room-temperature band gaps of 2.75, 2.92, 2.36, 2.37, and 2.26 eV for **I**, **II**, **III**, **IV**, and **V**, respectively, and also display strong photoluminescence. The thermal analysis data for all compounds are reported. The properties of these compounds are compared with those of the three-dimensional compounds CdS, CdSe, and CdTe, as well as those of the nanometer-sized CdQ clusters. A conceptual context is presented to connect all these different types of compounds.

Keywords
cadmium compounds · chalcogen compounds · crystal structure · dimensionality · photoluminescence

Introduction

The semiconducting, photoconducting, and light-emitting properties of CdS, CdSe, and CdTe have made them some of the most important members of the II–VI family of solids.[1] Recently, nanometer-sized "quantum dots"[2] and "nanowhiskers"[3] of these materials have been shown to display different properties from those of the bulk materials, such as blue-shifted band gaps, exciton confinement and stronger luminescence. Techniques such as encapsulation in zeolites,[4] preparation of quantum wells,[5] synthesis in micelles, surface alkylation to generate thiolate-terminated bonds,[6] and production of condensation polymers containing quantum dots[7] have been used to break up the II–VI compounds into nanometer-sized particles. While these techniques aim to reduce all of the dimensions of the II–VI crystals in order to achieve narrower electronic bands, we wondered whether the same electronic effects could be attained by reducing the *dimensionality* of the II–VI lattices. We chose to achieve this dimensional reduction of CdQ by the incorporation of A_2Q. The alkali metal polychalcogenide molten salt method can serve as an excellent route. Molten A_2Q_x salts allow the use of moderate temperatures (550–800 °C) and offer the possibility of forming metastable structures, with alkali metals incorporated into the lattice.[8] The materials thus formed can be extended structures of reduced dimensionality, or in some cases, discrete molecular ions. As a result of decreased Cd–Q connectivity, these compounds possess electronic band structures qualitatively mimicking those of quantum-sized particles. The latter display decreased connectivity at their surfaces, which account for a large number of the cluster atoms. Recently, we reported a blue-shifted band gap and bright luminescence in $K_2Cd_2S_3$,[9] which has a $(Cd_2S_3)_n^{2n-}$ framework with K^+-filled tunnels. By varying the synthetic conditions, we have produced other compounds in this system.

We reasoned that lessons learned in the so-called zero-dimensional "quantum dot" field could possibly be applied to lower-dimensional, bulk A/Cd/Q compounds. These ternary materials could display anisotropic $Cd_xQ_y^{z-}$ lattices with 3-D channeled or cave structures, 2-D, or 1-D structures. Such structures and concepts have been articulated before and, for example, 3-D cave structures have been proposed as inverse quantum "antidots".[10] Bulk materials with anisotropic structures that display blue-shifted band gaps (with respect to bulk CdS, CdSe, or CdTe), excitonic absorptions, strong luminescence, quantum confinement along certain crystallographic directions and homogeneous melting could be quite interesting, not only from a fundamental point of view but also in applications. Large single crystals of these materials are more easily accessible than bulk single crystals of quantum dots. We note, however, that the preparation of small quantum-dot single crystals of CdSe has been demonstrated.[11] In this context, these novel, low-dimensional materials could combine the advantages of both quantum dots and bulk solids.

In the last few years, the so-called "natural quantum well" compounds have been studied intensively. These compounds consist of perovskite-type layers of edge-sharing octahedra, with alkylammonium cations separating the layers. They are typified by $(C_{10}H_{21}NH_3)_2PbI_4$, $(CH_3NH_3)(C_{10}H_{21}NH_3)_2PbI_4$ and $(CH_3NH_3)PbI_3$.[12] These compounds display efficient luminescence, higher band gaps than PbI_2, and confined excitons. Exciton confinement has been attributed to both the finite thickness of the inorganic layers and the large difference in dielectric constant between these layers and the alkylammonium cations

[*] M. G. Kanatzidis, E. A. Axtell III, J.-H. Liao, Z. Pikramenou
Department of Chemistry and Center for Fundamental Materials Research
Michigan State University, East Lansing, MI 48824-1322 (USA)
Fax: Int. code +(517)353-1793

0947-6539/96/0206-0656 $ 15.00+.25/0

between them. This latter effect has been referred to as "dielectric confinement." The properties of these materials will be compared and contrasted with those of the $A_2Cd_3Q_4$ compounds.

We note a relative paucity of reported A/Cd/Q compounds, which include only Na_6CdS_4,[13a] Na_2CdS_2,[13b] and $Na_4Cd_3Se_5$.[13c] The first compound contains discrete $(CdS_4)^{6-}$ tetrahedra, while the second contains 1-D $(CdS_2)_n^{2n-}$ chains, and the third displays a layered structure. In this contribution, we report in detail the synthesis, characterization, and physicochemical properties of the new compounds $K_2Cd_3S_4$, $Rb_2Cd_3S_4$, $K_2Cd_3Se_4$, $Rb_2Cd_3Se_4$, and $K_2Cd_3Te_4$. We will discuss their structures and optical and spectroscopic properties with respect to property dependence on dimensionality.

Experimental Procedure

Materials: Cadmium metal was obtained from Johnson Matthey Electronics (Lot 17529), elemental sulfur from Spectrum Chemical (Lot EE597), both elemental selenium and tellurium from Aldrich (99.8%, Lot 04705CY), potassium metal (98%) from Aldrich, and rubidium metal, CdS (99.999%, Lot X14056), CdSe (99.995%, Lot 70624A-33-40WP1) and CdTe (99.999%, Lot 36312-G-(1-12)W) from Cerac.

Synthesis of K_2S, K_2Se and K_2Te: Potassium sulfide, potassium selenide, and potassium telluride were produced in liquid ammonia. In a nitrogen-filled glove box, the stoichiometric amounts of potassium and elemental chalcogen (S, Se, or Te) powder necessary to produce 20 g of starting material were loaded into a 250 ml round-bottomed flask. A Teflon stir bar was added and the flask closed to air with a glass adapter and valve. This apparatus was then attached to a Schlenk line, where approximately 150 ml of liquid ammonia was condensed under nitrogen, with stirring, into the dry-ice/acetone-cooled flask. After the flask had warmed to room temperature, the apparatus was held under vacuum for several hours and then heated with a hot-air gun to drive off any remaining ammonia. The apparatus was returned to the glove box, and the product was ground to a fine powder before use. The sulfide, selenide, and telluride powders were pale yellow, pale orange, and beige, respectively.

Synthesis of Rb_2S and Rb_2Se: In a nitrogen-filled glove box, rubidium metal was gently heated until molten. Approximately 10 g of the alkali metal was subsequently weighed into a three-necked, 500 ml round-bottomed flask. The center neck was closed with a glass adapter and valve, while the two outer necks were closed with ground glass stoppers. After the stoichiometric amount of elemental sulfur or selenium needed had been calculated, this was weighed from a stock in the glove box and placed in a clean, dry vial. The apparatus was then removed to a Schlenk line. Liquid ammonia was condensed under nitrogen into the dry-ice/acetone-cooled flask. After the flask had been half filled and swirled to dissolve the rubidium, a Teflon-coated stir bar was added through a side neck. The solution was then set stirring before the addition of the sulfur or selenium. Subsequently, the material was treated as above before use, resulting in pale yellow and pale orange powders of the sulfide and selenide, respectively. **Caution:** Potassium and rubidium are highly reactive! The flask residue was rinsed carefully with isopropyl alcohol to destroy any remaining alkali metal.

Synthesis of $K_2Cd_3S_4$: The reaction of K_2S (0.331 g, 3.0 mmol), Cd metal (0.056 g, 0.5 mmol), and elemental S (0.128 g, 4.0 mmol) was accomplished in a 3/8 in o.d. × 1/4 in i.d. × 3 in alumina thimble. After the powdered starting materials were loaded into the thimble, it was sealed inside a 13 mm o.d. × 11 mm i.d. carbon-coated quartz tube. The tube was placed in a computer-controlled furnace and heated to 600 °C for 2 d, followed by 5 °C h^{-1} cooling to 50 °C. Light yellow, transparent plates of $K_2Cd_3S_4$ were isolated with methanol under a nitrogen atmosphere. This compound is air- and water-stable, and is insoluble in common organic solvents. A yield of 60%, based on Cd, was typical. Semiquantitative microprobe analysis of a number of these crystals by SEM/EDS gave a composition of $K_{2.0}Cd_{2.8}S_{4.2}$.

$K_2Cd_3S_4$ was also prepared by a direct combination reaction at higher temperature. The mixture of K_2S (0.331 g, 3.0 mmol) and CdS (0.867 g, 6.0 mmol) was heated in a flat-bottomed alumina boat. The boat was sealed horizontally inside an evacuated, carbon-coated quartz tube (16 mm o.d. × 14 mm i.d.) and heated at 800 °C for 2 d, followed by cooling at 1 °C h^{-1} to 750 °C and 25 °C h^{-1} cooling to 50 °C. The 50% excess of K_2S promotes crystal growth, prevents formation of CdS and can be washed away with water, methanol, and ether. This reaction yielded centimeter-sized, polycrystalline plates.

Synthesis of $Rb_2Cd_3S_4$: Large yellow plates of $Rb_2Cd_3S_4$ were obtained by the reaction of Rb_2S (0.609 g, 3.0 mmol), Cd metal (0.056 g, 0.5 mmol), and elemental S (0.064 g, 2.0 mmol). This charge was first loaded into an alumina thimble, then sealed inside an evacuated, carbon-coated quartz tube. The tube was placed inside a computer-controlled furnace and heated at 800 °C for 3 d, followed by 10 °C h^{-1} cooling to 400 °C, 20 °C h^{-1} cooling to 50 °C and quenching to room temperature. The product was isolated with methanol under a nitrogen atmosphere. The compound is air- and water-stable. A yield of 50%, based on Cd, was typical. Semiquantitative analysis of a number of these crystals by SEM/EDS gave a composition of $Rb_{2.0}Cd_{3.2}S_{4.4}$.

Synthesis of $K_2Cd_3Se_4$: Large yellow plates of $K_2Cd_3Se_4$ were obtained by the reaction of K_2Se (0.236 g, 1.5 mmol), Cd metal (0.028 g, 0.25 mmol), and elemental Se (0.158 g, 2.0 mmol). This charge was first loaded into an alumina thimble, then sealed inside an evacuated, carbon-coated quartz tube. The tube was placed inside a computer-controlled furnace and heated at 650 °C for 2 d, followed by 5 °C h^{-1} cooling to 400 °C and quenching to room temperature. The product was isolated with methanol under nitrogen. The compound is insoluble in water and common organic solvents, but is sensitive to long exposure to air. A yield of 57%, based on Cd, was typical. Semiquantitative analysis of a number of these crystals by SEM/EDS gave a composition of $K_{2.0}Cd_{2.4}Se_{2.9}$.

Synthesis of $Rb_2Cd_3Se_4$: Dark yellow plates of $Rb_2Cd_3Se_4$ were obtained by the reaction of Rb_2Se (0.375 g, 1.5 mmol), Cd (0.028 g, 0.25 mmol), and elemental Se (0.118 g, 1.5 mmol). This charge was placed inside an alumina thimble, which was sealed inside a carbon-coated quartz tube under vacuum. The tube was heated inside a computer-controlled furnace at 650 °C for 2 d, followed by cooling at 5 °C h^{-1} to 200 °C, and finally quenching to room temperature. The product was isolated with methanol under nitrogen. The compound is insoluble in water and common organic solvents, but is sensitive to prolonged exposure to air. A yield of 52%, based on Cd, was typical. Semiquantitative analysis of a number of these crystals by SEM/EDS gave a composition of $Rb_{2.0}Cd_{3.6}Se_{4.8}$.

Synthesis of $K_2Cd_3Te_4$: Orange plates of $K_2Cd_3Te_4$ were obtained by the reaction of K_2Te (0.103 g, 0.5 mmol) and CdTe (0.360 g, 1.5 mmol). This charge was placed inside an alumina thimble, which was sealed inside a carbon-coated quartz tube under vacuum. This tube was heated at 800 °C in a computer-controlled furnace for 2 d, followed by cooling at 10 °C h^{-1} to 400 °C, and finally, at 25 °C h^{-1} to room temperature. The product was isolated with methanol under nitrogen. The compound is insoluble in water and common organic solvents, but is sensitive to exposure to air. A yield of 45%, based on CdTe, was typical. Here, the reaction was performed stoichiometrically to prevent decomposition of large amounts of K_2Te. Semiquantitative analysis of a number of these crystals by SEM/EDS gave a composition of $K_{2.0}Cd_{3.2}Te_{4.2}$.

Single Crystal X-Ray Diffraction: Single crystal X-ray diffraction data for $K_2Cd_3S_4$ and $Rb_2Cd_3Se_4$ were collected on a computer-controlled Nicolet (Siemens) P3F four-circle diffractometer ($Mo_{K\alpha}$ radiation, graphite-monochromated) at 20 °C. Cell parameters were determined by least-squares refinement of fifteen computer-centered reflections with $2\theta > 25°$. The intensity data were collected with the ω-scan technique. Single crystal X-ray diffraction data for $Rb_2Cd_3S_4$ and $K_2Cd_3Te_4$ were collected on a computer-controlled Nicolet P3V four-circle diffractometer ($Mo_{K\alpha}$ radiation, graphite-monochromated, $2\theta/\omega$-scan technique) at low temperature (−122 °C for $Rb_2Cd_3S_4$ and −80 °C for $K_2Cd_3Te_4$). Cell parameters were determined by least-squares refinement of eighteen computer-centered reflections with $12 < 2\theta < 40°$. None of the four crystals showed significant decay as judged by three check reflections measured every 150 reflections throughout their respective data sets. The space groups were determined from the systematic absences and intensity statistics. The structures were solved by the direct methods routine of SHELXS-86 [14] and refined by the full-matrix least-squares techniques of the TEXSAN package of crystallographic programs [15]. For $K_2Cd_3S_4$, $Rb_2Cd_3S_4$, and $Rb_2Cd_3Se_4$ an empirical absorption correction based on ψ-scans was applied to each data set, followed by a DIFABS [16] correction to the isotropically refined structure. For $K_2Cd_3Te_4$, only the DIFABS absorption correction was applied. For $K_2Cd_3S_4$, $Rb_2Cd_3Se_4$, and $K_2Cd_3Te_4$, all atoms were eventually refined anisotropically. For $Rb_2Cd_3S_4$, only the Rb and Cd atoms were refined anisotropically. All calculations were performed on a VAX Station 3100/76 computer. The complete parameters and details of the structure solution and refinement for the four compounds are given in Tables 1 and 2. The coordinates of all atoms, isotropic equivalent temperature factors, and their standard deviations are given in Tables 3, 4, 5, and 6. For $K_2Cd_3Se_4$, only the unit cell dimensions were determined: $a = 14.32(3)$, $b = 10.59(2)$, and $c = 6.79(1)$ Å. This cell and the atomic positions observed in $K_2Cd_3S_4$ (with Se substituted for S) were used to calculate the theoretical powder diffraction pattern for $K_2Cd_3Se_4$. Though preferred orientation was present, the observed powder pattern matched reasonably well with the calculated one.

The five compounds were examined by X-ray powder diffraction to check for phase purity and for identification. Powder patterns obtained on a Philips XRG-3000 powder diffractometer and a Rigaku rotating anode ($Cu_{K\alpha}$) X-ray powder diffractometer, Rigaku–Denki/*Rw* 400 *F*2 (Rotaflex), provided accurate d_{hkl} spacings and showed $K_2Cd_3S_4$, $Rb_2Cd_3S_4$, $K_2Cd_3Se_4$, $Rb_2Cd_3Se_4$, and $K_2Cd_3Te_4$ to be X-ray isomorphous. The calculated [17] and observed powder patterns of $K_2Cd_3S_4$ are given in Table 7, while the rest have been deposited with the supplementary material [32]. Further details of the crystal structure investigations may be obtained from the

Table 1. Summary of crystallographic data for $K_2Cd_3S_4$ and $Rb_2Cd_3S_4$.

	$K_2Cd_3S_4$	$Rb_2Cd_3S_4$
FW ($g\,mol^{-1}$)	543.67	543.67
color, habit	trans. yellow, plate	trans. lt. brown, plate
dimensions (mm)	$0.18\times0.20\times0.38$	$0.44\times0.26\times0.013$
a (Å)	13.880(4)	14.217(6)
b (Å)	10.247(3)	10.525(4)
c (Å)	6.608(1)	6.558(2)
V (Å^3)	939.8(7)	981(1)
space group	*Pnma* (no. 62)	*Pnma* (no. 62)
Z	4	4
ρ_{calcd} ($g\,cm^{-3}$)	3.84	4.31
$\mu(Mo_{K\alpha})$ (cm^{-1})	83.76	67.67
radiation [λ (Å)]	$Mo_{K\alpha}$ (0.71069)	$Mo_{K\alpha}$ (0.71069)
T (°C)	20	−122
scan type	ω	$\omega/2\theta$
scan rate (°min^{-1})	2.0–6.0	2.0
$2\theta_{max}$ (°)	54.8	50.1
min./max. absorption coeff.		
ψ scan correction	0.90/1.08	0.69/1.22
no. reflns measured	1103	1015
no. reflns $I>3\sigma(I)$	879	493
no. variables	49	38
R/R_w [a]	3.4%/4.2%	5.3%/4.3%
GoF	1.76	2.44

[a] $R=\sum(|F_o|-|F_c|)/\sum|F_o|$; $R_w=\{\sum w(|F_o|-|F_c|)^2/\sum w|F_o|^2\}^{1/2}$; $w=1/\sigma^2(F)$.

Table 2. Summary of crystallographic data for $Rb_2Cd_3Se_4$ and $K_2Cd_3Te_4$.

Formula	$Rb_2Cd_3Se_4$	$K_2Cd_3Te_4$
FW ($g\,mol^{-1}$)	824.01	925.83
color, habit	dark yellow, plate	orange, plate or rod
dimensions (mm)	$0.025\times0.18\times0.38$	$0.2\times0.05\times0.05$
a (Å)	14.749(7)	15.137(8)
b (Å)	11.012(4)	11.307(4)
c (Å)	6.802(3)	7.292(7)
V (Å^3)	1105(1)	1248(2)
space group	*Pnma* (no. 62)	*Pnma* (no. 62)
Z	4	4
ρ_{calcd} ($g\,cm^{-3}$)	4.95	4.93
$\mu(Mo_{K\alpha})$ (cm^{-1})	272.18	148.62
radiation (λ [Å])	$Mo_{K\alpha}$ (0.71069)	$Mo_{K\alpha}$ (0.71069)
T (°C)	20	−80
scan type	ω	$2\theta/\omega$
scan rate (°min^{-1})	2.0–6.0	2.0
$2\theta_{max}$ (°)	50.7	60.0
min./max. absorption coeff.		
ψ scan correction	0.94/1.57	0.67/1.25
no. reflns measured	1209	2121
no. reflns $I>3\sigma(I)$	740	1009
no. variables	49	49
R/R_w [a]	4.3%/4.4%	6.4/6.2
GoF	1.38	4.28

[a] $R=\sum(|F_o|-|F_c|)/\sum|F_o|$; $R_w=\{\sum w(|F_o|-|F_c|)^2/\sum w|F_o|^2\}^{1/2}$; $w=1/\sigma^2(F)$.

Table 3. Fractional atomic coordinates and B_{eq} [a] values for $K_2Cd_3S_4$ (estimated standard deviations in parentheses).

Atom	x	y	z	B_{eq}
Cd1	0.79603(7)	0.75	0.2236(1)	0.86(3)
Cd2	0.75168(4)	0.40831(6)	0.16226(8)	0.90(2)
K1	1.0	0.5	0.0	1.7(1)
K2	0.5315(2)	0.75	−0.0216(4)	1.7(1)
S1	0.8535(2)	0.75	−0.1307(4)	0.9(1)
S2	0.6417(2)	0.75	0.4321(4)	0.8(1)
S3	0.6348(1)	0.4672(2)	−0.1181(3)	0.74(6)

[a] B values for anisotropically refined atoms are given in the form of the isotropic equivalent displacement parameters, defined as $B_{eq}=(4/3)[a^2B(1,1)+b^2B(2,2)+c^2B(3,3)+ab(\cos\gamma)B(1,2)+ac(\cos\beta)B(1,3)+bc(\cos\alpha)B(2,3)]$.

Table 4. Fractional atomic coordinates and B_{eq} [a] values for $Rb_2Cd_3S_4$ (estimated standard deviations in parentheses).

Atom	x	y	z	B_{eq}
Cd1	0.2062(3)	0.25	0.2481(5)	0.5(1)
Cd2	0.2473(2)	0.5921(2)	0.1854(3)	0.55(8)
Rb1	0.0	0.5	0.0	1.0(2)
Rb2	0.4661(4)	0.25	−0.0244(7)	1.0(2)
S1	0.1515(9)	0.25	−0.109(2)	0.4(2) [b]
S2	0.3564(9)	0.25	0.460(2)	0.5(2) [b]
S3	0.3615(5)	0.5376(6)	−0.099(1)	0.3(1) [b]

[a] B values for anisotropically refined atoms are given in the form of the isotropic equivalent displacement parameters, defined as $B_{eq}=(4/3)[a^2B(1,1)+b^2B(2,2)+c^2B(3,3)+ab(\cos\gamma)B(1,2)+ac(\cos\beta)B(1,3)+bc(\cos\alpha)B(2,3)]$. [b] Isotropic temperature factors.

Table 5. Fractional atomic coordinates and B_{eq} [a] values for $Rb_2Cd_3Se_4$ (estimated standard deviations in parentheses).

Atom	x	y	z	B_{eq}
Cd1	0.7935(1)	0.75	0.2585(2)	1.52(7)
Cd2	0.7450(1)	0.9059(1)	0.6910(2)	1.53(5)
Rb1	0.5	1.0	0.5	2.8(1)
Rb2	0.5366(2)	0.75	−0.0234(4)	2.3(1)
Se1	0.8480(2)	0.75	−0.1039(3)	1.41(9)
Se2	0.6402(2)	0.75	0.4637(3)	1.35(9)
Se3	0.8625(1)	0.9632(1)	0.4105(2)	1.33(6)

[a] B values for anisotropically refined atoms are given in the form of the isotropic equivalent displacement parameters, defined as $B_{eq}=(4/3)[a^2B(1,1)+b^2B(2,2)+c^2B(3,3)+ab(\cos\gamma)B(1,2)+ac(\cos\beta)B(1,3)+bc(\cos\alpha)B(2,3)]$.

Table 6. Fractional atomic coordinates and B_{eq} [a] values for $K_2Cd_3Te_4$ (estimated standard deviations in parentheses).

Atom	x	y	z	B_{eq}
Te1	0.8654(2)	0.25	0.0765(5)	1.2(1)
Te2	0.6445(2)	0.25	−0.3698(5)	1.3(1)
Te3	0.6324(1)	0.4685(2)	0.1094(3)	1.21(7)
Cd1	0.7023(2)	0.25	0.2698(6)	1.4(1)
Cd2	0.7562(2)	0.4032(2)	−0.1619(4)	1.36(9)
K1	0.5	0.5	0.5	2.2(5)
K2	0.4651(8)	0.25	−0.028(2)	2.2(5)

[a] B values for anisotropically refined atoms are given in the form of the isotropic equivalent displacement parameters, defined as $B_{eq}=(4/3)[a^2B(1,1)+b^2B(2,2)+c^2B(3,3)+ab(\cos\gamma)B(1,2)+ac(\cos\beta)B(1,3)+bc(\cos\alpha)B(2,3)]$.

Fachinformationzentrum Karlsruhe, 76344 Eggenstein-Leopoldshafen (Germany), on quoting the depository number CSD-59268.

Semiquantitative Microprobe Analysis: Semiquantitative microprobe analysis was performed on a JEOL JSM-35C scanning electron microscope (SEM) and a JEOL JSM-6400 SEM equipped with a Noran energy-dispersive spectroscopy (EDS) system. Data acquisition was performed with an accelerating voltage of 20 kV. Compositions given are the average of several 30 s acquisitions.

Optical Spectroscopy: A Shimadzu UV-3101PC double-beam, double-monochromator spectrophotometer was used to measure the room-temperature optical diffuse reflectance spectra of the five compounds. The methods used to collect the reflectance data and convert it to absorbance values have been described elsewhere [18]. We obtained the band gap values by extrapolating the linear regions of each $(\alpha/S)^2$ versus energy plot to $(\alpha/S)^2=0$ [19]. These values are estimated to be accurate to ±0.03 eV. Single-crystal absorption spectra were obtained on a Hitachi U-6000 Microscopic FT spectrophotometer mounted on an Olympus BH2-UMA microscope. Crystals lying on a glass slide were positioned over the light source and the transmitted light was detected from above.

Photoluminescence Spectroscopy: Photoluminescence spectra for $K_2Cd_3S_4$, $Rb_2Cd_3S_4$, $K_2Cd_3Se_4$, $Rb_2Cd_3Se_4$, and $K_2Cd_3Te_4$ were obtained on a Spex Fluorolog-2 F111A1 spectrofluorimeter. Excitation wavelengths were chosen from a 150 W xenon arc lamp by means of a single grating spectrometer. This spectrometer

0947-6539/96/0206-0658 $ 15.00+.25/0 Chem. Eur. J. 1996, 2, No. 6

Table 7. Calculated and observed powder patterns for $K_2Cd_3S_4$.

$h\,k\,l$ (%)	d_{calcd} (Å)	d_{obs} (Å)	$I/I_{o,obs}$
2 0 0	6.94	7.00	100
1 1 1	5.16	5.19	2
2 0 1	4.79	4.80	3
4 0 0	3.47	3.49	45
4 1 0	3.29	3.31	14
3 2 1	3.05	3.06	21
2 0 2	2.98	3.00	17
2 1 2	2.86	2.88	5
2 3 1	2.78	2.79	23
3 0 2	2.69	2.70	19
3 3 1	2.54	2.55	3
2 4 0	2.403	2.426	4
4 3 1	2.284	2.293	17
6 0 1	2.183	2.191	5
5 0 2	2.125	2.134	17
5 3 1	2.048	2.059	3
6 2 1	2.009	2.015	13
2 2 3	1.943	1.957	3
7 1 1, 6 1 2	1.867	1.872	8
6 3 1, 1 3 3	1.840	1.841	12
8 0 0	1.735	1.739	18
3 3 3, 6 4 0	1.719	1.720	11
2 6 0, 8 1 1	1.658	1.661	14
8 3 0	1.547	1.552	3
4 6 2, 10 0 0	1.390	1.390	5
9 3 1, 6 6 0	1.375	1.375	3
10 1 1	1.347	1.351	10

was equipped with a 1200 groove mm^{-1} diffraction grating and 5 nm band pass slits. The sample compartment was equipped with a vertically mounted quartz liquid-nitrogen Dewar. Emitted light was collected in the "front face" mode, 22.5° away from the incident beam. Emission wavelengths were selected with a single grating spectrometer equipped with a 1200 groove mm^{-1} diffraction grating and 1.0 nm band pass slits. The signal was detected with a Hamamatsu R928 photomultiplier. Excitation spectra were corrected for lamp intensity by comparison with a quantum counter reference detector loaded with rhodamine B. Powdered samples were loaded into 3 mm quartz tubing and sealed under vacuum (approx. 1.0×10^{-4} mbar).

Differential Thermal Analysis (DTA): Thermal analysis was performed on a Shimadzu DTA-50 differential thermal analyzer. High-quality crystals were selected from the reaction product and ground. Approximately 15–20 mg of each material was loaded into a 2.0 mm i.d. × 3.0 mm o.d. quartz tube with a flattened bottom and sealed under a vacuum of less than 1×10^{-4} mbar. Since $K_2Cd_3S_4$ reacts with glass at temperatures higher than 500 °C, the quartz tube was first carbon-coated by the pyrolysis of acetone. Such a tube filled with 20 mg of Al_2O_3 powder was used as the reference in this case. The samples of $Rb_2Cd_3S_4$ and $K_2Cd_3Te_4$ were treated in a similar manner. An uncoated tube was used for both reference and sample in the cases of the two selenide compounds. Heating and cooling rates of 10 °C min^{-1} were used. Typically, the samples showed an endothermic peak upon heating and an exothermic peak upon cooling. The temperature associated with each thermal event was assigned to the melting and recrystallization, respectively, of each compound. Comparisons between powder patterns taken before and after heating were made to establish whether each compound melted with or without decomposition.

Results and Discussion

Description of the Structure: These compounds are composed of anionic cadmium chalcogenide layers situated perpendicular to the *a* axis (Fig. 1). Inspection of the layer quickly reveals that $Cd_3Q_4^{2-}$ clusters are the fundamental building blocks in this new structure type. These $Cd_3Q_4^{2-}$ clusters take the form of truncated cubes, shown in Figure 2. A three-coordinate Q atom assumes the apex of the cluster by bonding to three Cd atoms. The remaining three Q atoms each bond to two Cd atoms in the cube-like cluster and one Cd in an adjacent cluster. These bonds result in the formation of three distorted rhombi, with one point common to all three. The cuboidal clusters are arranged in rows along the *c* axis. Within each row, the clusters point in the same direction. Rows of clusters are arranged side by side, pointing in

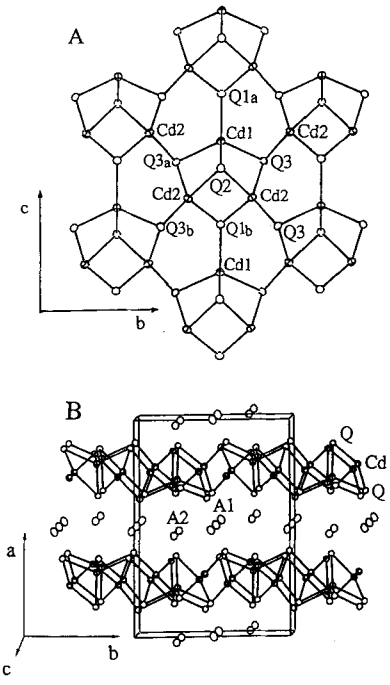

Fig. 1. A) The structure of one $(Cd_3S_4)_n^{2n-}$ layer. B) The three-dimensional structure of $K_2Cd_3S_4$ looking down the crystallographic *c* axis.

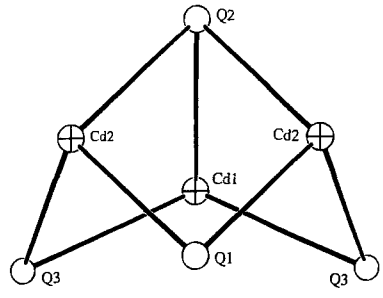

Fig. 2. The $Cd_3S_4^{2-}$ defect cubane unit.

opposite directions as the *b* axis is traversed. Each cluster has six neighbors, two of which point in the same direction and four of which point in the opposite direction. The crystallographically determined Cd–Q distances, tabulated in Table 8, are compar-

Table 8. Selected bond lengths (Å) up to 4.0 Å for $K_2Cd_3S_4$, $Rb_2Cd_3S_4$, $Rb_2Cd_3Se_4$, and $K_2Cd_3Te_4$ (standard deviations in parentheses) [a].

	$K_2Cd_3S_4$	$Rb_2Cd_3S_4$	$Rb_2Cd_3Se_4$	$K_2Cd_3Te_4$
Cd1–Cd2	3.3867(9)	3.380(4)	3.481(2)	4.002(3)
Cd2–Cd2	3.244(2)	3.324(4)	3.434(2)	3.465(5)
Cd1–Q1$_a$	2.474(2)	2.47(1)	2.593(3)	2.770(6)
Cd1–Q2	2.547(3)	2.55(1)	2.658(3)	2.844(5)
Cd1–Q3	2.640(2)	2.633(7)	2.760(2)	2.931(3)
Cd2–Q1$_b$	2.576(2)	2.58(1)	2.684(2)	2.856(4)
Cd2–Q2	2.672(2)	2.67(1)	2.780(2)	2.960(4)
Cd2–Q3$_a$	2.536(2)	2.537(8)	2.654(2)	2.823(4)
Cd2–Q3$_b$	2.494(2)	2.502(8)	2.612(2)	2.781(4)
A1–Q1	3.383(2)	3.475(8)	3.620(2)	3.698(2)
A1–Q2	3.261(2)	3.341(8)	3.452(2)	3.529(2)
A1–Q3	3.159(2)	3.311(8)	3.475(2)	3.501(3)
A2–Q1	3.366(4)	3.57(1)	3.764(4)	3.69(1)
A2–Q2	3.366(4)	3.54(1)	3.648(4)	3.62(1)
A2–Q3	3.295(3)	3.407(7)	3.519(2)	3.559(6)
A2–Q3	3.336(3)	3.415(8)	3.563(3)	3.675(9)

[a] The estimated standard deviations in the mean bond length are calculated by the equations $\sigma l = \{\sum_n (l_n - l)^2/n(n-1)\}^{1/2}$, where l_n is the length of the *n*th bond, l the mean length, and *n* the number of bonds.

Table 9. Selected bond angles (°) for $K_2Cd_3S_4$, $Rb_2Cd_3S_4$, $Rb_2Cd_3Se_4$, and $K_2Cd_3Te_4$ (standard deviations in parentheses) [a].

	$K_2Cd_3S_4$	$Rb_2Cd_3S_4$	$Rb_2Cd_3Se_4$	$K_2Cd_3Te_4$
$Q1_a$-Cd1-Q2	141.6(1)	141.5(5)	139.8(1)	138.1(2)
$Q1_a$-Cd1-Q3	104.93(6)	104.3(2)	103.99(6)	105.3(1)
Q2-Cd1-Q3	95.26(6)	95.6(2)	96.72(6)	96.6(1)
$Q3_a$-Cd1-$Q3_b$	114.91(9)	116.2(3)	116.6(1)	114.9(2)
$Q1_b$-Cd2-Q2	103.54(6)	101.3(2)	102.06(6)	106.71(9)
$Q1_b$-Cd2-$Q3_b$	111.79(7)	113.6(3)	113.55(7)	110.9(1)
$Q1_b$-Cd2-$Q3_a$	100.08(7)	100.0(3)	98.98(6)	97.9(1)
Q2-Cd2-$Q3_a$	94.77(7)	95.1(3)	96.34(7)	96.5(1)
Q2-Cd2-$Q3_b$	106.97(8)	108.1(3)	108.71(8)	108.6(1)
$Q3_a$-Cd2-$Q3_b$	135.08(4)	133.5(1)	132.56(5)	133.37(9)
Cd2-Q1-Cd2	78.06(9)	80.3(4)	79.55(9)	74.7(1)
Cd1-Q2-Cd2	80.90(8)	80.7(3)	79.56(8)	78.8(1)
Cd2-Q2-Cd2	74.79(8)	77.1(3)	76.28(8)	71.7(1)
Cd1-Q3-Cd2	81.72(6)	81.6(2)	79.99(7)	79.6(1)
Q1-A1-Q1	180.00	180.00	180.00	180.00
Q1-A1-Q2	78.61(6)	78.4(2)	77.19(6)	76.67(7)
Q1-A1-Q2	101.39(6)	101.6(2)	102.81(6)	103.33(7)
Q1-A1-Q3	76.55(6)	72.8(2)	72.96(5)	78.03(7)
Q1-A1-Q3	103.45(6)	107.2(2)	107.04(5)	101.97(7)
Q2-A1-Q2	180.00	180.00	180.00	180.00
Q2-A1-Q3	99.41(6)	102.0(2)	101.48(5)	96.90(7)
Q2-A1-Q3	80.59(6)	78.0(2)	78.52(5)	83.10(7)
Q3-A1-Q3	180.00	180.00	180.00	180.00
Q1-A2-Q2	72.1(3)	72.4(3)	71.30(7)	68.1(2)
Q1-A2-Q2	160.0(1)	158.5(3)	157.1(1)	157.2(4)
Q1-A2-Q3	71.45(7)	68.2(2)	67.20(7)	71.1(2)
Q1-A2-Q3	112.59(6)	103.1(2)	103.08(6)	101.0(2)
Q2-A2-Q3	121.64(7)	121.0(2)	119.10(6)	119.8(3)
Q2-A2-Q3	93.89(8)	96.0(2)	96.08(7)	92.3(3)
Q2-A2-Q3	69.65(6)	71.8(2)	73.36(5)	71.1(2)
Q2-A2-Q3	88.55(7)	86.3(2)	86.51(6)	88.8(2)
Q2-A2-Q3	123.1(1)	125.3(3)	127.6(1)	126.9(1)
Q3-A2-Q3	160.22(9)	158.2(2)	157.41(8)	158.8(3)
Q3-A2-Q3	76.57(6)	76.4(4)	74.97(6)	74.34(8)
Q3-A2-Q3	83.7(1)	81.8(8)	82.44(9)	84.5(3)

[a] The estimated standard deviations in the mean bond angles are calculated by the equations $\sigma l = \{\sum_n (l_n - l)^2/n(n-1)\}^{1/2}$, where l_n is the angle between the nth bond, l the mean angle, and n the number of angles.

able to other known cadmium chalcogenides.[9, 11–13, 20] The presence of the three four-membered rings within the defect cube results in a rather distorted tetrahedral coordination for cadmium (Table 9). The alkali metal counterions display distorted octahedral coordination spheres (Fig. 3). One of the cations, A2, directly faces a pocket formed by the sulfur atoms of the cuboidal $Cd_3Q_4^{2-}$ units. The face of the octahedron shared with the cluster is denoted by the dotted lines. The Cd atoms are in distorted tetrahedral coordination, while the Q atoms are exclusively three-coordinate. This differs from bulk CdS, CdSe, and CdTe, in which both Cd and the chalcogen are in regular tetrahedral coordination. Conversely, large numbers of three-coordinate chalcogen atoms are found on the surfaces of quantum-sized particles. These particles, with their higher surface-to-volume ratio, differ from the bulk compounds by displaying a higher percentage of surface atoms with more distorted and/or lower connectivity. In a sense, then, the $A_2Cd_3Q_4$ compounds could be viewed as being formed by peeling the surfaces from quantum-sized particles, rolling them flat, and stacking them together with A^+ to balance the negative charge. The negative charges exist as "dangling" bonds in CdQ nanoparticles, which can be balanced by capping with terminal thiol ligands. Viewing the $A_2Cd_3Q_4$ compounds this way provides an interesting new conceptual framework in which to rationalize some of their properties, namely, blue-shifted band gaps and brighter luminescence than in the bulk II–VI compounds.

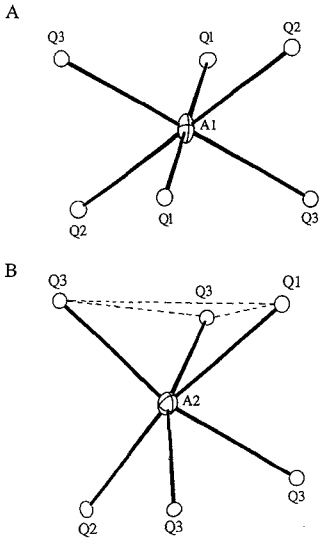

Fig. 3. The coordination sphere of the alkali ions K^+ or Rb^+, designated as A1 and A2 for the two crystallographic sites.

A molecular analog of the $Cd_3S_4^{2-}$ cluster of $K_2Cd_3S_4$ is contained in $(NMe_4)[Cd_3(SC_6H_2iPr_3)_7]\cdot C_5H_{12}$.[21] This compound has longer Cd–S bond lengths about the apical S atom (ranging from 2.709(7) to 2.800(8) Å) than those in $K_2Cd_3S_4$ (2.547(3) to 2.672(2) Å). Other bonds around the periphery of the defect cube are more similar, ranging from 2.488(9) to 2.56(1) Å in $(NMe_4)[Cd_3(SC_6H_2iPr_3)_7]\cdot C_5H_{12}$ and from 2.536(2) to 2.640(2) Å in $K_2Cd_3S_4$. No luminescence studies were reported for this compound. To the best of our knowledge, no selenium or tellurium analogs of this compound have been reported.

The $K_2Cd_3S_4$ structure type represents a fourth structure type with the $A_2M_3Q_4$ formula, where M = Zn, Cd, or Hg. In both $Na_2Hg_3S_4$[22] and $A_2Hg_3Q_4$ (A = K, Cs and Q = S, Se),[23] Hg is present in two different coordination environments. In $Na_2Hg_3S_4$, there are both linear and trigonal planar Hg atoms. The structure as a whole consists of highly corrugated layers. In $K_2Hg_3S_4$, $(Hg_3S_4)_n^{2n-}$ linear chains are separated by K^+. These chains consist of tetrahedral HgS_4 units linked together by linear Hg. The third structure type, $Cs_2Zn_3S_4$,[24] features a defect anti-PbO structure, where one quarter of the metal atoms have been removed, resulting in eight-membered Zn_4S_4 rings. Both $Cs_2Zn_3S_4$ and $K_2Cd_3S_4$ are layered, with trigonal pyramidal coordination about the chalcogen. $K_2Cd_3S_4$ displays significantly distorted tetrahedra, with S-M-S angles ranging from 96 to 138°, while this range is only 92–114° in $Cs_2Zn_3S_4$. These two structure types are compared in Figure 4.

It is interesting that the $Cs_2Zn_3S_4$ structure type seems to form with a larger ratio of alkali metal to transition metal radius ($Rb_2Zn_3S_4$, $Cs_2Mn_3S_4$, and $Cs_2Co_3S_4$ are all isostructural).[25] This radius ratio varies from 2.05 to 2.49 for the $Cs_2Zn_3S_4$-type compounds but it is significantly smaller for the $K_2Cd_3S_4$-type compounds, varying from 1.45 to 1.60.[26] This observation suggests that the counterion-to-metal radius ratio alone may be responsible for the stabilization of these structures.

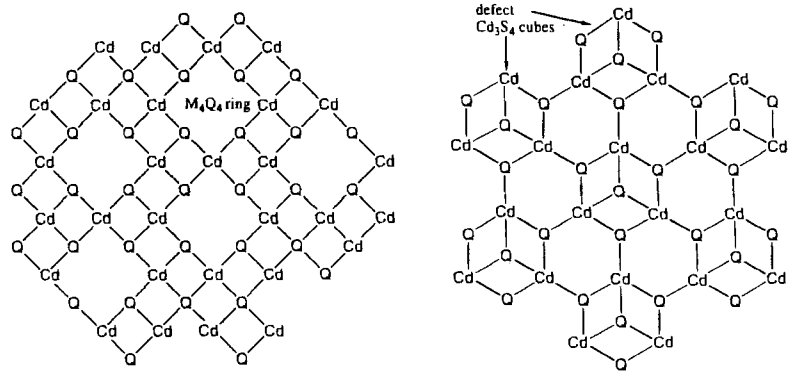

Fig. 4. Comparison of an idealized $(Zn_3S_4)_n^{2n-}$ layer and an idealized $(Cd_3S_4)_n^{2n-}$ layer.

0947-6539/96/0206-0660 $ 15.00+.25/0 Chem. Eur. J. 1996, 2, No. 6

Optical Spectroscopy: All $A_2Cd_3Q_4$ compounds are lighter in color than their corresponding CdQ parent compounds. The absorption spectra display steep absorption edges that are the result of charge-transfer excitations between a Q p-like valence band and a Cd 5s-like conduction band, similar to those occurring in the CdQ binaries (Figs. 5 and 6). Table 10 summarizes all

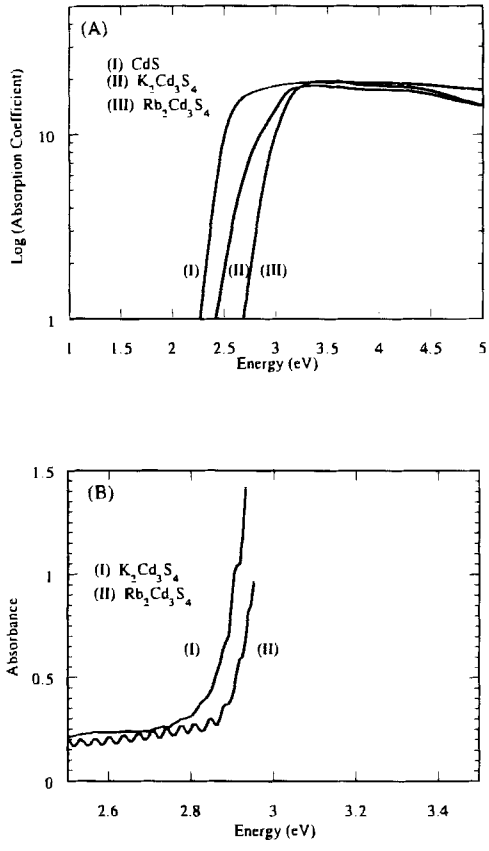

Fig. 5. A) Solid-state absorption spectra of CdS, $K_2Cd_3S_4$, and $Rb_2Cd_3S_4$. B) Single crystal absorption spectra of $K_2Cd_3S_4$ and $Rb_2Cd_3S_4$. The interference pattern observed below the band gap results from the finite thickness of the specimens and their high refractive index relative to air.

the optical absorption and emission (vide infra) properties observed for the compounds reported here. The band gaps increase from 2.44 eV in CdS[19] to 2.75 eV in $K_2Cd_3S_4$ and 2.92 eV in $Rb_2Cd_3S_4$; from 1.74 eV in CdSe[19] to 2.36 and 2.37 eV for $K_2Cd_3Se_4$ and $Rb_2Cd_3Se_4$, respectively, and from 1.5 eV in CdTe[19] to 2.26 eV in $K_2Cd_3Te_4$. The absorption spectra of the parent II–VI compounds are displayed in Figures 5 and 6 for

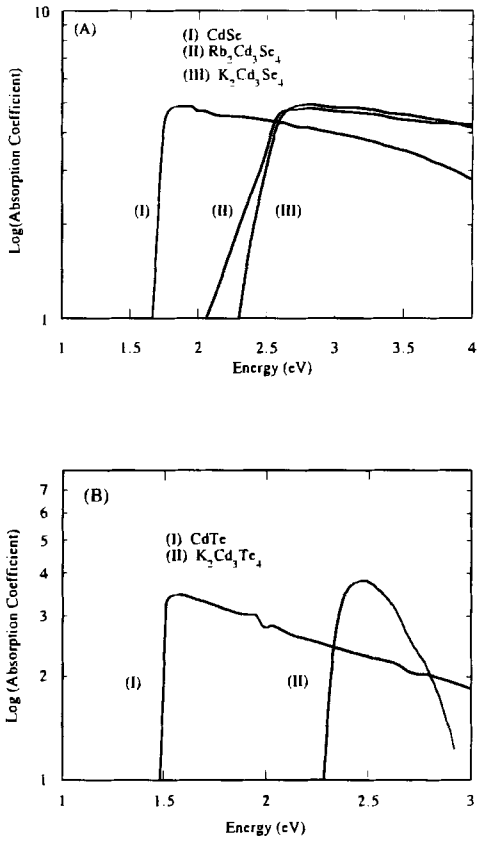

Fig. 6. Solid-state absorption spectra of: A) CdSe, $K_2Cd_3Se_4$, and $Rb_2Cd_3Se_4$; B) CdTe, $K_2Cd_3Te_4$.

comparison. We note that the band gaps of CdS, CdSe, and CdTe are direct. The similarity of their absorption spectra with those of the $A_2Cd_3Q_4$ compounds and the observation of bright luminescence would indicate that the band gaps of the ternaries are also most likely direct. The single crystal transmission spectra of $K_2Cd_3S_4$ and $Rb_2Cd_3S_4$ are in good agreement with the diffuse reflectance spectra obtained from the powder samples, giving band gaps of 2.82 and 2.92 eV for $K_2Cd_3S_4$ and $Rb_2Cd_3S_4$, respectively (Fig. 7). These band gaps are consistent with the colors of the materials. The two sulfides are pale yellow, the two selenides are a deeper yellow and the telluride is orange in color. This dramatic effect is attributed to the breakup of the parent structure, which results in frameworks of reduced dimensionality (at least in one direction in this case). Band dispersion in these materials is much narrower than in the bulk CdQ compounds and along the *a* axis is almost zero, approaching discrete electronic levels. This is qualitatively what occurs in quantum-sized particles.[27]

Table 10. Summary of spectroscopic data for $K_2Cd_3S_4$, $Rb_2Cd_3S_4$, $K_2Cd_3Se_4$, $Rb_2Cd_3Se_4$, and $K_2Cd_3Te_4$ (energies in eV).

	$K_2Cd_3S_4$	$Rb_2Cd_3S_4$	$K_2Cd_3Se_4$	$Rb_2Cd_3Se_4$	$K_2Cd_3Te_4$	
E_g of parent CdQ	2.44	2.44	1.74	1.74	1.5	
E_g of $A_2Cd_3Q_4$	2.75	2.92	2.36	2.37	2.26	
E_g increase	0.31	0.48	0.62	0.63	0.76	
effective size [a]	45–50	45–50	19–23	19–23	<30	
emission of parent CdQ	weak, 1.63	weak, 1.63	none	none	1.59, Ar^+ laser, 10 K	
RT emission of $A_2Cd_3Q_4$	strong, 1.92	weak, 2.41	strong, 2.00	none	none	none
77 K emission of $A_2Cd_3Q_4$	strong, 2.41	weak, 1.92	strong, 1.98	strong, 1.92	strong, 2.01	strong, 2.04
band edge of 77 K excitation spectrum	3.31, 3.12	3.30	2.53	2.59	2.39	
emission maximum of 77 K excitation spectrum	3.17, 2.80	2.96	2.75	2.75	2.49	

[a] Diameter (Å) of a CdQ quantum-sized particle that would display a similar band (HOMO–LUMO) gap.

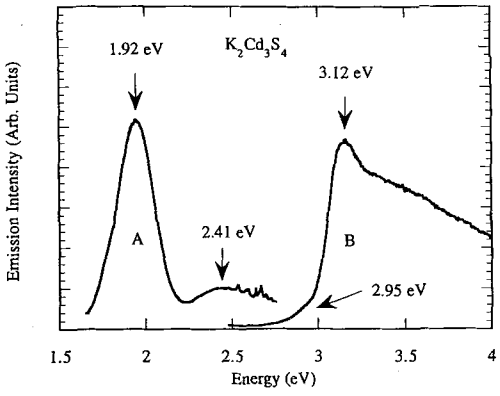

Fig. 7. Room-temperature emission spectra of $K_2Cd_3S_4$. A) $E_{exc} = 3.12$ eV and B) $E_{det} = 1.92$ eV.

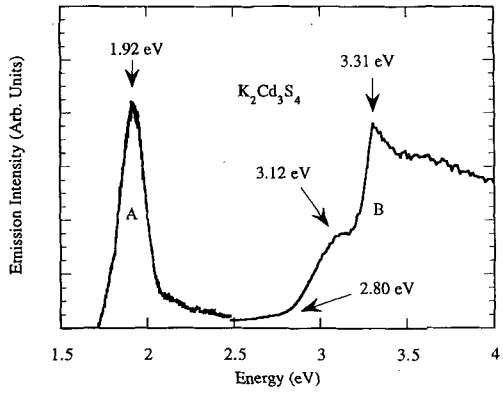

Fig. 8. Photoemission spectra of $K_2Cd_3S_4$ at 77 K. A) $E_{exc} = 3.12$ eV and B) $E_{det} = 1.92$ eV.

In the case of $K_2Cd_3Te_4$, air sensitivity made accurate band-gap determination difficult. A black material began coating the surface soon after exposure to air. The absorption spectrum therefore displays two steps, consistent with a mixture. Unfortunately, the band gap of interest was the higher one. To obtain the band gap, the x axis was artificially raised so that it intersected with the steepest drop from $K_2Cd_3Te_4$. The validity of this approach was tested by obtaining the correct band gap of 2.44 eV for CdS[17] from a mixture of CdTe and CdS. Further credence for this band-gap determination was gained from the absorption edge of the excitation spectrum (see below).

Similar results have been seen in the Cat^+/Pb/I system, where the compounds display band gaps larger than the parent, PbI_2.[10] The band gaps depend on dimensionality (3-D < bilayer < monolayer), cation size/shape, and halide.

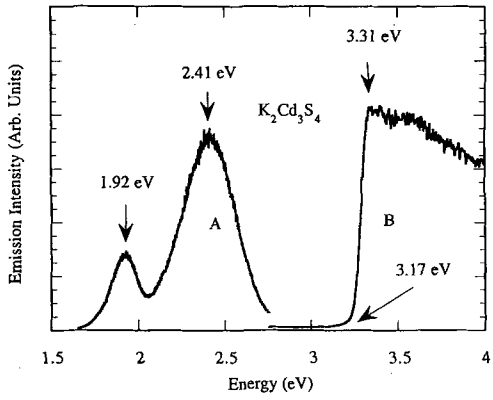

Fig. 9. Photoemission spectra of $K_2Cd_3S_4$ at 77 K. A) $E_{exc} = 3.31$ eV and B) $E_{det} = 2.41$ eV.

Photoluminescence Spectroscopy: All five compounds exhibit intense photoluminescence when excited with light above the band gap. The sulfides emit strongly even at room temperature, while the selenides and the telluride must be cooled to 77 K, Table 10.

$K_2Cd_3S_4$: With an excitation line of 3.12 eV (397 nm), this compound shows intense red emission at room temperature, with a maximum at 1.92 eV (646 nm) (Fig. 7). Also, a small emission peak is observed at 2.41 eV (514 nm). Since the room-temperature band gap of $K_2Cd_3S_4$ is 2.75 eV (451 nm), light emission probably arises from mid-gap states. The room-temperature excitation spectrum of $K_2Cd_3S_4$, detected at 1.92 eV, displays a maximum at 3.12 eV (397 nm), which falls rapidly to zero at approximately 2.95 eV (420 nm). This value is close in energy to the band gap determined by optical absorption. Upon cooling to 77 K, a fascinating result is obtained. First, with an excitation line of 3.12 eV (397 nm), the same (but much sharper) red emission (1.92 eV, 646 nm) is obtained (see Fig. 8). Upon collecting an excitation profile with $E_{det} = 1.92$ eV ($\lambda_{det} = 646$ nm), two intensity drops are observed, with edges at 3.31 eV (375 nm) and 3.12 eV (397 nm). When the excitation line is changed to 3.31 eV (375 nm), a change of only 0.19 eV (22 nm), a drastic color change in the emission from red to intense yellow is observed. The intensity of the 1.92 eV (646 nm) peak is dramatically reduced and the peak at 2.41 eV (514 nm) becomes very strong (see Fig. 9). Finally, an excitation profile recorded with $E_{det} = 2.41$ eV ($\lambda_{det} = 514$ nm) shows only the band with an edge at 3.31 eV (375 nm). Here, the emission falls to zero by 3.17 eV (391 nm).

The possibility that the two emissions could arise from an impure sample at 77 K was eliminated by positioning a large single crystal of this material in the beam. In an attempt to check for orientation effects on the 77 K luminescence, data were collected with the plate both perpendicular and parallel to the incident beam. The emission spectra were reproduced in both orientations. The thin nature of the platelike crystals made the parallel measurement rather unreliable. To the unaided eye, emission at the edge of the plate and at grain boundaries appeared brighter than when the beam impinged on a smooth transparent portion of the plate at right angles.

The emission data suggest that the nature of the band structure in $K_2Cd_3S_4$ may be rather complex. Since band structure is three-dimensional in nature,[27, 28] it is possible that two different band gaps exist in the anisotropic $K_2Cd_3S_4$, depending on the crystallographic direction. Viewed parallel to the layers, the compound could appear almost molecular, owing to the 4 Å thickness of the $(Cd_3Q_4)_x^{2x-}$ layers. The band gap in this direction would therefore be expected to be larger compared with those in the other two directions, where the Cd–S bonding is infinitely extended. More work is needed to determine the nature of the band structure in this compound.

A spectral orientation dependence was observed in the layered compounds of the system Cat^+/Pb/I with polarized reflection spectroscopy.[10c] When the optical field is perpendicular to the layers, the compounds reflect light more strongly than in the parallel direction. A similar dependence is expected for the $A_2Cd_3Q_4$ compounds.

0947-6539/96/0206-0662 $ 15.00+.25/0 Chem. Eur. J. 1996, 2, No. 6

$Rb_2Cd_3S_4$: With an excitation line of 3.18 eV (390 nm), this compound shows intense red emission at room temperature, with a maximum at 2.00 eV (621 nm), see Figure 10. Since the room-temperature band gap of $Rb_2Cd_3S_4$ is 2.92 eV (425 nm),

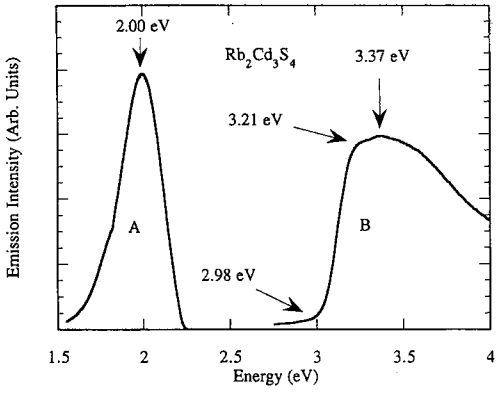

Fig. 10. Room-temperature emission spectra of $Rb_2Cd_3S_4$. A) $E_{exc} = 3.18$ eV and B) $E_{det} = 2.00$ eV.

this emission probably arises from mid-gap states. The room-temperature excitation spectrum of $Rb_2Cd_3S_4$, detected at 2.00 eV (621 nm), displays a maximum at 3.37 eV (368 nm), which falls rapidly to zero at approximately 2.98 eV (416 nm). This is in good agreement with the band gap determined by optical absorption (see above). At 77 K, $Rb_2Cd_3S_4$ shows the same red luminescence, with a maximum at 1.98 eV (625 nm), when excited with 3.30 eV (375 nm) light (Fig. 11). In contrast

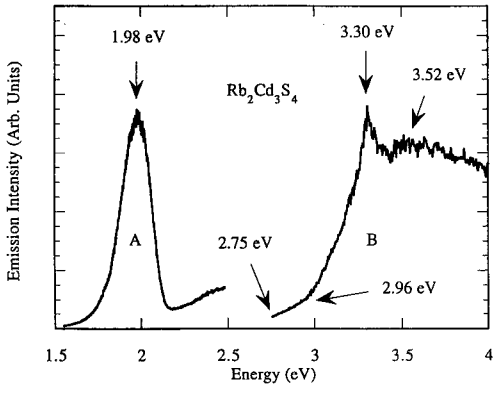

Fig. 11. Photoemission spectra of $Rb_2Cd_3S_4$ at 77 K. A) $E_{exc} = 3.30$ eV and B) $E_{det} = 1.98$ eV.

to $K_2Cd_3S_4$, the 77 K excitation spectrum of $Rb_2Cd_3S_4$, detected at 1.98 eV (625 nm), reveals only one edge. The shape of the edge is somewhat different than for the other materials, with a gradual drop from 3.30 to 2.96 eV (375 to 419 nm) and an even more shallow drop to 2.75 eV (451 nm).

For comparison purposes, photoluminescence spectra for 99.999% CdS were obtained. This bulk material displays only weak emission at 1.63 eV (760 nm) when cooled to 77 K. Intense emission can be obtained from the II–VI compounds, but it requires activation with dopants such as Mn and Cu. In stark contrast, the $A_2Cd_3Q_4$ compounds emit strongly without intentional attempts to activate them. Apparently, fragmentation of the dense three-dimensional lattice of the CdQ compounds is the cause of this strong emission.

A compound with optical properties comparable to $K_2Cd_3S_4$ and $Rb_2Cd_3S_4$ has been reported by Herron and co-workers.[6] The thiol-capped $Cd_{32}S_{14}(SC_6H_5)_{36}\cdot DMF_4$ is a cluster with a 15 Å CdS core. In the solid state at 6.5 K, this compound emits green light with a maximum of 2.38 eV (520 nm) when excited with a 3.88 eV (320 nm) line. The excitation spectrum, while the 2.38 eV (520 nm) emission was monitored, shows absorption bands at 3.81 eV (325 nm) and 3.23 eV (384 nm), with a weak shoulder at 2.85 eV (435 nm). $K_2Cd_3S_4$, $Rb_2Cd_3S_4$, and $Cd_{32}S_{14}(SC_6H_5)_{36}\cdot DMF_4$ all show a significant blue shift from the expected absorption edge of 2.44 eV (508 nm) for CdS. Brus and co-workers[27] have calculated the effect of cluster size on the band gap/first excited state for CdS in small clusters. The band gap values of $K_2Cd_3S_4$ and $Rb_2Cd_3S_4$ correspond to an effective size of 45–50 Å. In other words, the bulk compounds reported here possess attributes that might be expected from nanometer-sized CdS clusters of 45–50 Å size.

$K_2Cd_3Se_4$ and $Rb_2Cd_3Se_4$: No room-temperature emission is visible or detectable for $K_2Cd_3Se_4$ or $Rb_2Cd_3Se_4$. At 77 K, $K_2Cd_3Se_4$ shows red luminescence with a maximum at 1.92 eV (642 nm) when excited with 2.88 eV (428 nm) light (Fig. 12).

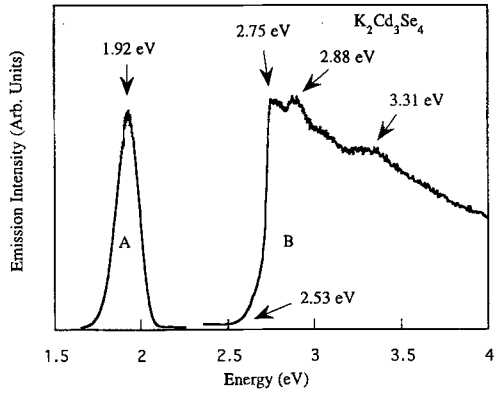

Fig. 12. Photoemission spectra of $K_2Cd_3Se_4$ at 77 K. A) $E_{exc} = 2.88$ eV and B) $E_{det} = 1.92$ eV.

The 77 K excitation spectrum, detected at 1.92 eV (642 nm), reveals two features at 3.31 and 2.88 eV (375 and 428 nm). The edge of the steep drop occurs at 2.75 eV (450 nm) and falls to zero by 2.53 eV (480 nm). This value is just 0.12 eV higher than the room-temperature band gap of 2.36 eV. This slight energy increase is to be expected, considering that the band gaps of semiconductors increase at lower temperatures.

When excited with 2.75 eV (451 nm) light at 77 K, $Rb_2Cd_3Se_4$ also emits red light, with a maximum at 2.0 eV (619 nm) (Fig. 13). The 77 K excitation spectrum, detected at 2.0 eV (619 nm), shows a feature at 2.90 eV (429 nm). A sharp peak with a maximum at 2.75 eV (451 nm) precedes the precipitous drop in intensity. The intensity drops to zero by 2.59 eV (480 nm). In similar fashion to $K_2Cd_3Se_4$, this value is slightly higher than the room temperature band gap of 2.37 eV.

For comparison purposes, CdSe was also examined under the same conditions. No luminescence was visible or detectable. $K_2Cd_3Se_4$ and $Rb_2Cd_3Se_4$ possess superior light emitting qualities compared with CdSe, apparently as a result of fragmentation of the dense 3-D structure of CdSe. Bawendi and co-workers have recently developed the preparation of nearly monodisperse CdSe clusters ranging in size from approximately 12 to approximately 115 Å.[29] As the size decreases, the absorp-

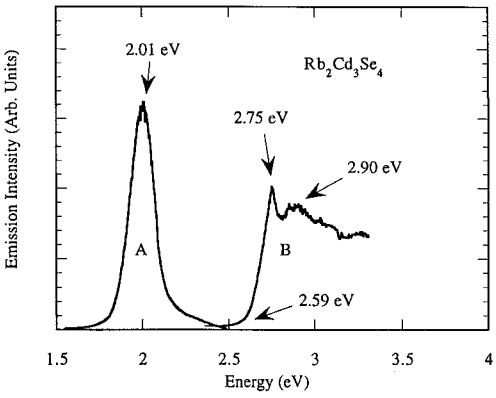

Fig. 13. Photoemission spectra of $Rb_2Cd_3Se_4$ at 77 K. A) $E_{exc} = 2.75$ eV and B) $E_{det} = 2.01$ eV.

tion edge moves the bulk value of 1.74 eV (708 nm) for the 115 Å clusters to a value of 2.92 eV (425 nm) for the 12 Å clusters. In this case, experimental evidence indicates that $K_2Cd_3Se_4$ and $Rb_2Cd_3Se_4$ behave in a similar manner to 19–23 Å clusters of CdSe.

$K_2Cd_3Te_4$: No room-temperature emission is visible or detectable for $K_2Cd_3Te_4$. When excited with 2.49 eV (497 nm) light at 77 K, the compound emits orange light, with a maximum at 2.04 eV (609 nm) (Fig. 14). The 77 K excitation spec-

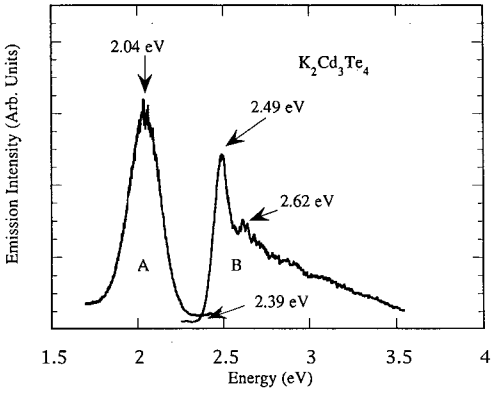

Fig. 14. Photoemission spectra of $K_2Cd_3Te_4$ at 77 K. A) $E_{exc} = 2.49$ eV and B) $E_{det} = 2.04$ eV.

trum, detected at 2.00 eV (619 nm), shows a sharp peak with a maximum at 2.49 eV (497 nm), followed by a precipitous drop in intensity, suggesting a band gap of 2.39 eV (525 nm). This value is only slightly higher than the room-temperature band gap value, obtained with optical absorption, see above.

In comparison, CdTe emits at 1.59 eV when excited with an Ar^+ laser at 10 K.[30] The advantages of $K_2Cd_3Te_4$ over CdTe with respect to light emission are clear. Use of $K_2Cd_3Te_4$ negates the need for a laser, merely requiring a Xe lamp as the light source. Though the CdTe nanocluster work is not as well developed as for the lighter analogs, Bawendi and co-workers found that 30 Å clusters of CdTe possess an absorption edge of 1.91 eV (650 nm). The significantly larger band gap of $K_2Cd_3Te_4$ (2.26 eV) suggests that it possesses properties that could only be realized in a much smaller cluster of CdTe.

It is noteworthy that all of the compounds display emission maxima between 1.92 and 2.04 eV. To explain this observation, attention must be paid to the valence and conduction bands of these materials. The valence band probably consists of mainly Q p-like bonding orbitals. Relative energy increases are expected as these orbitals change from S 3p-like to Se 4p-like to Te 5p-like. On the other hand, the conduction band is mainly Cd 5s-like antibonding orbitals, and as such may not change much in going from S to Se to Te. The emission is probably from the conduction band to a deep trap resulting from Cd vacancies or an impurity level lying between the gap. The energy differences between orbitals based on Cd should remain close to constant, consistent with the observed results. Support for Cd vacancies as the origin of the mid-gap states comes from the observation of brighter luminescence from the edges of the large plate of $K_2Cd_3S_4$. The lack of room-temperature emission in the heavier selenide and telluride analogs is caused by nonradiative thermal relaxation mediated by these mid-gap states and is consistent with the proposed band picture above.

Unlike the Cat^+/Pb/I compounds, so far no confined excitons have been observed in the $A_2Cd_3Q_4$ compounds. One contribution to exciton confinement in the Cat^+/Pb/I compounds comes from the low dielectric constant of the organic cations between the layers, resulting in smaller screening of the Coulomb interaction of the electron and the hole.[12] The $A_2Cd_3Q_4$ compounds contain layers separated only by a monolayer of A^+ cations, resulting in more screening of the Coulomb interaction and weaker confinement. Of course, confinement may still be possible at very low temperatures.

Thermal Properties: Differential thermal analysis (DTA) was used to evaluate the thermal properties of these materials. Upon heating, $K_2Cd_3S_4$, $Rb_2Cd_3S_4$, $K_2Cd_3Se_4$, and $Rb_2Cd_3Se_4$ showed endothermic peaks centered at 816, 912, 784, and 908 °C, respectively. These peaks correspond to congruent melting transitions and are followed by exothermic crystallization peaks upon cooling at 764, 879, 756, and 883 °C, respectively. X-ray powder patterns were used for compound identification.

Compound $K_2Cd_3Te_4$ exhibited two endothermic peaks upon heating, at 522 and 690 °C, which were followed by two exothermic peaks, at 679 and 488 °C, upon cooling. After the experiment, transparent orange plates and some black material were visible under microscopic examination. The eight weak peaks observed in the powder pattern could be assigned to $K_2Cd_3Te_4$. It is tempting to assign the 690/679 °C pair of peaks to melting and recrystallization, respectively, of $K_2Cd_3Te_4$. The 522/488 °C pair of peaks belong to an as yet unidentified impurity.

Structure/Property Relationships: Although at first glance the relationship between a nanometer-sized CdS cluster and $K_2Cd_3S_4$ (or a related ternary compound with a low-dimensional Cd/Q framework) seems remote, the origin of the wider band gap relative to bulk CdQ is common. For example, in both nanometer-sized CdS clusters and $K_2Cd_3S_4$, the widening of the band gap is achieved by narrowing the width of the valence and conduction bands. In quantum dots, it is achieved by reducing the number of atoms involved in bonding to small, definable numbers. In the $A_2Cd_3Q_4$ compounds, bulk numbers of atoms are still involved in bonding. It is the incorporation of A_2Q, which causes the attendant reduction in coordination number of the chalcogen, that results in the dimensional reduction of the structure and in reduced orbital overlap that leads to narrowing of the bands. While in nanometer-sized clusters confinement is achieved in all three dimensions by the small physical size of the cluster, in the $A_2Cd_3Q_4$ compounds quantum confinement might be expected only in crystallographic directions where band dispersion is minimal (e.g., perpendicular to the *a* axis).

0947-6539/96/0206-0664 $ 15.00+.25/0 Chem. Eur. J. 1996, 2, No. 6

Both CdQ and $A_2Cd_3Q_4$ are members of a homologous series of the type $(A_2Q)_x(CdQ)_y$. With increasing A_2Q content, the dimensionality changes from a dense 3-D structure in CdQ to 2-D in the $A_2Cd_3Q_4$ compounds. Then, anomalously, the dimensionality changes to a 3-D channel structure for $K_2Cd_2S_3$.[9] Further increases in A_2Q content lead to a 1-D chain structure for A_2CdQ_2,[31] finally ending with the zero-dimensional, isolated molecules of CdS_4^{6-},[11] the end member of this series. A simple diagram that notes the structural evolution from bulk CdS to CdS_4^{6-} molecules is seen in Figure 15. The

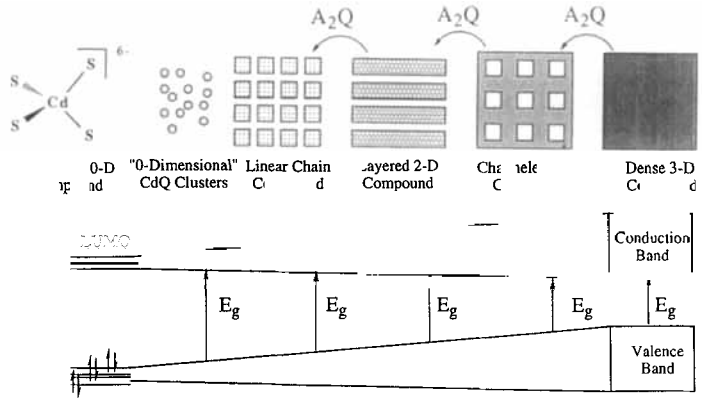

band gaps should increase on moving to the lower dimensional materials, as is indeed observed not only in the compounds reported here, but in the $Cat^+/Pb/I$ compounds[12] and other A/Cd/Q compounds as well. For example, the band gap of Rb_2CdSe_2[31] is higher than those of $Rb_2Cd_3Se_4$ and $K_2Cd_3Se_4$.

The properties of $K_2Cd_2S_3$ may fall within this framework. While the higher K_2S content in the formula relative to $K_2Cd_3S_4$ would suggest that the material should be of lower dimensionality than $K_2Cd_3S_4$, the compound displays a 3-D, channeled Cd/S lattice. Now, given that this structure is 3-D, one would expect it to possess a lower band gap with respect to $K_2Cd_3S_4$. Interestingly, though the band gap of 2.89 eV for $K_2Cd_2S_3$ is slightly greater than the band gap of 2.75 eV for $K_2Cd_3S_4$, it is slightly smaller than the band gap of 2.92 eV for $Rb_2Cd_3S_4$. This example illustrates a potential pitfall in evaluating "dimensionality" in intermediate members of the $(A_2Q)_x(CdQ)_y$ family. One may not necessarily go only by the bulk dimensionality observed in the structure, but also by the extent of framework atom connectivity, that is, the coordination number of Cd and Q. Given that the coordination number of Cd is always four, close attention must be paid to the connectivity of the chalcogen. Ignoring the ionic A–Q interactions, the coordination number of the chalcogen is reduced from 4 in CdQ through 3 in $A_2Cd_3Q_4$ and 2 in A_2CdQ_2 to 1 in A_6CdQ_4. Since $K_2Cd_2S_3$ contains two three-coordinate sulfur atoms and one two-coordinate sulfur atom, the average coordination number for sulfur is 2.67, actually smaller than the 3 seen in $K_2Cd_3S_4$. This result suggests that both the overall, macroscopic dimensionality of the material and the extent of framework connectivity at the atomic level affect the properties of these materials. In other words, these two factors go hand in hand, though in some cases they could be divergent. As explained above, this is not inconsistent with the ideas discussed here.

Conclusion

The syntheses, structure, optical absorption, emission, and thermal properties of $K_2Cd_3S_4$, $Rb_2Cd_3S_4$, $K_2Cd_3Se_4$, $Rb_2Cd_3Se_4$, and $K_2Cd_3Te_4$ have been described here. Four of the compounds melt without decomposition. These compounds feature an unusual $(Cd_3Q_4)_n^{2n-}$ layer separated by A^+ cations. They display blue-shifted band gaps and strong emission relative to the parent binaries; this is attributed to their reduced dimensionality. This paper attempts to broaden the scope of the study of property dependence on quantum confinement to other kinds of materials. While a large amount of work has been performed with physically small semiconductor fragments, this work makes an important connection between these clusters and related bulk solid-state compounds with low-dimensional frameworks, which appear to mimic the physically small clusters.[10]

The concepts developed in this paper and elsewhere[9, 10] may aid in band-gap modification in other systems. For instance, the synthesis of a broken-up structure where the parent compound has a low-to-zero band gap could result in materials with intermediate band gaps of potential use in infrared detection or solar energy conversion. Further characterization of ternary or quaternary materials already in the literature should reveal relationships to their parent binaries similar to those highlighted in this work, as is the case in the $Cat^+/Pb/I$ system. Thinking in the context presented here could not only bring many new and interesting materials to light, but could also result in new lines of experimentation with known materials.

Acknowledgment: We thank Professor Daniel G. Nocera and Eric Saari for discussions and help with excitation and emission instrumentation in the early stages of this work. This research was made possible with funding from NSF Grant DMR-95-27347. M. G. K. is an A. P. Sloan Foundation Fellow and a Camille and Henry Dreyfus Teacher Scholar (1993–95).

Received: October 12, 1995 [F226]

[1] R. H. Bube, *Photoconductivity of Solids*, Wiley, New York, **1960**.
[2] a) R. Rossetti, R. Hull, J. M. Gibson, L. E. Brus, *J. Chem. Phys.* **1985**, *82(1)*, 552–559; b) G. C. Lisensky, R. L. Penn, C. J. Murphy, A. B. Ellis, *Science* **1990**, *248*, 840–843; c) L. Spanhel, M. A. Anderson, *J. Am. Chem. Soc.* **1990**, *112*, 2278–2284; d) M. L. Steigerwald, A. P. Alivisatos, J. M. Gibson, T. D. Harris, R. Kortan, A. J. Muller, A. M. Thayer, T. M. Duncan, D. C. Douglass and L. E. Brus, *ibid.* **1988**, *110*, 3046–3050; e) A. Henglein, *Top. Curr. Chem.* **1987**, *143*, 115–180; f) H. Weller, *Angew. Chem. Int. Ed. Engl.* **1993**, *32*, 41–53; g) Y. Wang, N. Herron, *J. Phys. Chem.* **1988**, *92*, 4988–4994; h) N. Herron, Y. Wang, H. Eckert, *J. Am. Chem. Soc.* **1990**, *112*, 1322–1326.
[3] J. D. Klein, R. D. Herrick, II, D. Palmer, M. D. Sailor, *Chem. Mater.* **1993**, *5*, 902–904.
[4] a) M. E. Benchley, M. T. Weller, *Angew. Chem. Int. Ed. Engl.* **1993**, *32*, 1663–1665; b) N. Herron, Y. Wang, M. M. Eddy, G. D. Stucky, D. E. Cox, K. Moller, T. Bein, *J. Am. Chem. Soc.* **1989**, *111*, 530–540.
[5] C. Weisbuch, B. Vinter, *Quantum Semiconductor Structures*, Academic Press, New York, **1991**.
[6] N. Herron, J. C. Calabrese, W. E. Farneth, Y. Wang, *Science* **1993**, *259*, 1426–1428.
[7] H. Noglik, W. J. Pietro, *Chem. Mater.* **1995**, *7*, 1333–1336.
[8] a) M. G. Kanatzidis, *Chem. Mater.* **1990**, *2*, 353–363; b) M. G. Kanatzidis, A. C. Sutorik, *Prog. Inorg. Chem.* **1995**, *93*, 151–205.
[9] E. A. Axtell III, J.-H. Liao, Z. Pikramenou, Y. Park, M. G. Kanatzidis, *J. Am. Chem. Soc.* **1993**, *115*, 12191–2.
[10] a) M. A. Reed, *Sci. Am.* **1993**, 118–123; b) G. A. Ozin, *Adv. Mater.* **1992**, *4*, 612–649; c) C. L. Bowes, G. A. Ozin, *Adv. Mater.* **1996**, *8*, 13–28; d) G. A. Ozin, *Supramol. Chem.* **1995**, *6*, 125–134; e) G. A. Ozin, *Materials Chemistry, an Emerging Subdiscipline*, in *Advances in Chemistry, ACS Symp. Ser.* **1995**, *245*, 91–120.
[11] C. B. Murray, C. R. Kagan, M. G. Bawendi, *Science* **1995**, *270*, 1335–1338.
[12] a) T. Ishihara, J. Takahashi, T. Goto, *Phys. Rev. B.* **1990**, *42*, 11099–11107; b) G. C. Papavassiliou, A. P Patsis, D. J. Lagouvardos, L. B. Koutselas, *Syn. Met.* **1993**, *55–57*, 3889–3894; c) X. Hong, T. Ishihara, A. V. Nurmikko, *Phys. Rev. B.* **1992**, *45*, 6961–6964; d) T. Ishihara, J. Takahashi, T. Goto, *Solid State Commun.* **1989**, *69*, 933–936; e) G. C. Papavassiliou, J. B Koutselas, D. J. Lagouvardos, *Z. Naturforsch.* **1993**, *48b*, 1013–1014; f) B. R. Vincent,

K. N. Robertson, T. S. Camaron, O. Knop, *Can. J. Chem.* **1987**, *65*, 1042–1046; g) S. S. Nagapetyan, Y. I. Dolzhenko, E. R. Arakelova, V. M. Koshkin, Y. T. Struchkov, V. E. Shklover, *Russ. J. Inorg. Chem.* **1988**, *33*, 1614–1618; h) A. Poglitsch, D. Weber, *J. Chem. Phys.* **1987**, *87*, 6373–6378; i) C.-Q. Xu, H. Sakakura, T. Kondo, S. Takeyama, N. Miura, Y. Takahashi, K. Kumata, R. Ito, *Solid State Commun.* **1991**, *79*, 249–253; j) C.-Q. Xu, T. Kondo, H. Sakakura, K. Kumata, Y. Takahashi, R. Ito, *ibid.* **1991**, *79*, 245–248; k) M. Era, S. Morimoto, T. Tsutsui, S. Saito, *Syn. Met.* **1995**, *71*, 2013–2014.

[13] a) K. O. Klepp, W. Bronger, *Rev. Chim. Miner.* **1983**, *20 (4–5)*, 682–688; b) I. R. Polyvyannyi, V. A. Lata, L. P. Ivakina, V. I. Antonyuk, *Russ. J. Inorg. Chem.* **1981**, *26 (4)*, 561–563; c) M. A. Ansari, J. A. Ibers, *J. Solid State Chem.* **1993**, *103*, 293–297.

[14] G. M. Sheldrick in *Crystallographic Computing 3* (Eds.: G. M. Sheldrick, C. Kruger, R. Doddard), Oxford University Press, Oxford, England, **1985**; pp. 175–189.

[15] TEXSAN: Single Crystal Structure Analysis Software, Version 5.0; Molecular Structure Corp., The Woodlands, TX 77381, **1981**.

[16] N. Walker, D. Stuart, *Acta Cryst.* **1983**, *39A*, 158.

[17] D. K. Smith, M. C. Nichols, M. E. Zolensky, POWD10: A Fortran IV Program for Calculating X-Ray Powder Diffraction Patterns, Version 10. Pennsylvania State University, **1983**.

[18] T. J. McCarthy, S.-P. Ngeyi, J.-H. Liao, D. C. DeGroot, J. Schindler, C. R. Kannewurf, M. G. Kanatzidis, *Chem. Mater.* **1993**, *5*, 331–340.

[19] J. I. Pankove in *Optical Processes in Semiconductors*, Dover, New York, **1975**.

[20] a) W. Becker, H. D. Lutz, *Mater. Res. Bull.* **1978**, *13*, 907–911; b) O. P. Agnihotri, A. K. Paturi, *Thin Solid Films* **1983**, *108*, 313–317; c) V. Chab, B. A. Orlowski, J. Bak-Misiuk, P. Dzonkowski, *Acta Phys. Pol.* **1985**, *67A*, 429–432; d) A. S. Pashinkin, R. A. Sapozhnikov, *Sov. Phys. Crystallogr.* **1962**, *7*, 501–502; e) M. G. Williams, R. D. Tomlinson, M. J. Hampshire, *Solid State Commun.* **1969**, *7*, 1831–1832; f) I. Dima, D. Borsan, *Phys. Status Solidi* **1967**, *23*, K113–K115.

[21] K. Tang, A. Li, X. Jin, Y. Tang, *J. Chem. Soc. Chem. Commun.* **1991**, 1590–91.

[22] K. O. Klepp, *J. Alloys Compd.* **1992**, *182*, 281–288.

[23] M. G. Kanatzidis, Y. Park, *Chem. Mater.* **1990**, *2*, 99.

[24] W. Bronger, U. Hendriks, *Rev. Chim. Miner.* **1980**, *17*, 555–560.

[25] W. Bronger, P. Böttcher, *Z. Anorg. Allg. Chem.* **1972**, *390*, 1–12.

[26] Ionic radii were taken from: N. N. Greenwood, A. Earnshaw, *Chemistry of the Elements*, Pergamon, Elmsford, NY, **1984**.

[27] L. E. Brus, *J. Phys. Chem.* **1986**, *90*, 2555–2560.

[28] D. Long, *Energy Bands in Semiconductors*, Interscience, New York, **1968**.

[29] C. B. Murray, D. J. Norris, M. G. Bawendi, *J. Am. Chem. Soc.* **1993**, *115*, 8706–8715.

[30] X. Huang, G. Lin, Y. Jing, *J. Lumin.* **1988**, *40 & 41*, 337–378.

[31] E. A. Axtell III, M. G. Kanatzidis, unpublished results.

[32] The following supplementary material is available from the correspondence author: calculated and observed powder patterns of $Rb_2Cd_3S_4$, $K_2Cd_3Se_4$, $Rb_2Cd_3Se_4$, and $K_2Cd_3Te_4$, anisotropic thermal parameters, bond lengths and angles of all atoms for $K_2Cd_3S_4$, $Rb_2Cd_3S_4$, $Rb_2Cd_3Se_4$, and $K_2Cd_3Te_4$, listings of calculated and observed structure factors for $K_2Cd_3S_4$, $Rb_2Cd_3S_4$, $Rb_2Cd_3Se_4$, and $K_2Cd_3Te_4$ (46 pages).

0947-6539/96/0206-0666 $ 15.00+.25/0